

Real-Time Damage Detection in Fiber Lifting Ropes Using Convolutional Neural Networks

Tuomas Jalonen, Mohammad Al-Sa'd, *Senior Member, IEEE*, Roope Mellanen, Serkan Kiranyaz, *Senior Member, IEEE*, and Moncef Gabbouj, *Fellow, IEEE*

Abstract—The health and safety hazards posed by worn crane lifting ropes mandate periodic inspection for damage. This task is time-consuming, prone to human error, halts operation, and may result in the premature disposal of ropes. Therefore, we propose using deep learning and computer vision methods to automate the process of detecting damaged ropes. Specifically, we present a novel vision-based system for detecting damage in synthetic fiber rope images using convolutional neural networks (CNN). We use a camera-based apparatus to photograph the lifting rope's surface, while in operation, and capture the progressive wear-and-tear as well as the more significant degradation in the rope's health state. Experts from Konecranes annotate the collected images in accordance with the rope's condition; normal or damaged. Then, we pre-process the images, design a CNN model in a systematic manner, evaluate its detection and prediction performance, analyze its computational complexity, and compare it with various other models. Experimental results show the proposed model outperforms other techniques with 96.4% accuracy, 95.8% precision, 97.2% recall, 96.5% F1-score, and 99.2% AUC. Besides, they demonstrate the model's real-time operation, low memory footprint, robustness to various environmental and operational conditions, and adequacy for deployment in industrial systems.

Index Terms—Computer vision, damage detection, deep learning, fiber rope, industrial safety.

I. INTRODUCTION

TRADITIONAL industries are transitioning to smart manufacturing under the Industry 4.0 paradigm [1], [2]. This transition allows the use of recent advances in artificial intelligence and computer vision to increase productivity and improve manufacturing safety [3], [4]. Nonetheless, lifting heavy payloads is still a major health and safety hazard in many manufacturing environments [5]. For example, cranes such as the one shown in Fig. 1 can move objects weighing several metric tons; hence, inspecting its ropes for damage is paramount to prevent serious accidents, injuries, and additional costs [6]. More specifically, lifting ropes are major points of

This work was funded by Konecranes Plc as part of Business Finland and DIMECC Intelligent Industrial Data Program. (*Corresponding author: Tuomas Jalonen.*)

Tuomas Jalonen and Moncef Gabbouj are with the Faculty of Information Technology and Communication Sciences, Tampere University, 33720 Tampere, Finland (e-mail: tuomas.jalonen@tuni.fi; moncef.gabbouj@tuni.fi).

Mohammad Al-Sa'd is with the Faculty of Medicine, University of Helsinki, 00014 Helsinki, Finland (e-mail: mohammad.al-sad@helsinki.fi) and the Faculty of Information Technology and Communication Sciences, Tampere University, 33720 Tampere, Finland mohammad.al-sad@tuni.fi).

Roope Mellanen is with Konecranes Plc, 05830 Hyvinkää, Finland (e-mail: roope.mellanen@konecranes.com).

Serkan Kiranyaz is with the Department of Electrical Engineering, Qatar University, 2713 Doha, Qatar (e-mail: mkiranyaz@qu.edu.qa).



Fig. 1. The fiber rope cranes used in this work. Photos are published with permission from Konecranes [7].

failure that require periodic inspection and replacement [8]. However, manual inspection procedures are labor intensive, time consuming, subjective, and often require halting the production process [9], [10], [11]. Therefore, we propose a novel real-time damage detection system for synthetic fiber lifting ropes based on deep learning and computer vision techniques.

The main contributions of this paper are:

- Developing the first fiber lifting rope image dataset.
- Proposing a deep learning based system for detecting damage in fiber lifting rope images.
- Designing an industrial solution that achieves high performance with a light memory footprint.

Lifting ropes are commonly manufactured from steel wires or lately using synthetic fibers such as polyethylene [12]. Synthetic lifting ropes have many benefits over traditional steel wire ropes. For example, they demonstrate higher resistance to corrosion, do not require greasing, and are easier to install [13]. Moreover, despite their higher purchase price, synthetic fiber ropes are lightweight which allows utilizing smaller cranes; leading to cost reductions [14]. However, synthetic ropes, just as steel wires, do suffer from wear-and-tear and get damaged over time. Common damage types in fiber ropes are: strand cuts, abrasion, melting, compression damage, pulled strands and inconsistent diameter. In contrast to steel wires which tend to break from the inside [15], synthetic rope damages manifest on the rope's surface and can be visually inspected by an expert [14]. Currently, monitoring the condition of synthetic fiber ropes is performed manually by inspectors following the ISO-9554 standard [9], [10]. Although it is the standard practice, this procedure is cumbersome, discontinuous in time, interrupts operation, and may result in the premature disposal of ropes [11]. Therefore, automatic

damage detection by leveraging the recent advancements in computer vision, image processing, and deep learning techniques is needed [14]. On the one hand, image processing and related feature extraction methods utilize expert knowledge and attempt to characterize damage in rope images similar to the ones identified by expert inspectors [16]. These techniques generally perform well in a controlled environment, but they poorly integrate the varying conditions and operations found in a real-life setting e.g., noise, lighting conditions, oil residue, and dust [17], [18]. On the other hand, deep learning tools discard the notion of hand-crafted features by learning abstractions that maximize the detection of damaged ropes. In fact, they yield discriminatory features without predisposition to the standard markings and can accommodate a wider range of environmental and/or operational conditions [17]. Therefore, deep learning techniques are more suited to detect damage in synthetic fiber rope images compared to engineering-based feature extraction methods.

The construct of damage indicators in fiber ropes was first articulated in [11] where changes in the rope's width and length were found to be important. This particular finding was verified in [19] using computer vision and thermal imaging; however, explicit identification for damaged ropes was not performed. In fact, detecting damage in synthetic fiber rope images has received less attention in the literature compared to steel wire cables. Fortunately, these detection techniques are suitable for adoption due to the similarity between the two problems; they both deal with detecting damaged yarns or strands in rope images. For instance, the health condition of balancing tail ropes was monitored in [20] using a convolutional neural network (CNN). The rope image was captured and then fed to the CNN model to classify its health state as either normal, or if it suffers from one out of eight common damage types. Moreover, a CNN-based approach was designed in [21] to detect surface defects in steel wire rope images. The model classified the acquired images into normal, broken, or damaged, and achieved a 99.7% overall accuracy. The same problem was tackled in [22] using support vector machines trained with texture-based hand-crafted features. The proposed system achieved a 93.3% classification accuracy and it was further improved in [23] to reach 95.9%. Nonetheless, the limited sample size and the reliance on hand-crafted features hampered robustness in noisy environments. This was evidenced in [24] which showed that the model accuracy drops to 80.5% when training/testing with a different dataset. Moreover, the utility of CNNs combined with image processing techniques was shown to increase the accuracy of the model in [22] from 93.3% to 95.5% [18]. This has motivated us to design a CNN-based solution for detecting damage in synthetic fiber rope images. However, our proposed solution will be developed to have both high performance and low computational requirements, allowing for easy integration into industrial systems and efficient deployment [25].

The rest of this paper is organized as follows: section II describes our methodology for building the experimental setup, collecting data, designing the damage detection system, and evaluating its performance. Afterwards, we present and discuss the system's performance and compare it to various

other models in section III. Finally, section IV concludes the paper and suggests topics for future research.

II. METHODOLOGY

The proposed fiber rope damage detection system is overviewed in Fig. 2 and consists of the following stages:

- 1) Setup an experimental apparatus with a three-camera circular array to photograph the ropes' surface area.
- 2) Collect the captured images and label them as normal or damaged according to the ropes' health condition.
- 3) Preprocess the collected images to enhance contrast and down-sample to reduce computational complexity.
- 4) Split the pre-processed images into train and test sets in a 5-fold cross-validation fashion.
- 5) Train and test a classification model on the train and test folds, respectively, and repeat for every data split.
- 6) Evaluate and analyze the model's fold-averaged performance using various metrics.

The design process undertaken in this work is governed by the following requirements:

- High performance in detecting damaged ropes and robustness to different environmental and operational conditions.
- Lightweight for implementation and deployment.
- Remote sensing by neither interfering with the crane operation nor the rope structure.
- Modularity to facilitate maintenance, upgrades, and compatibility with IoT and edge devices.

The remaining subsections discuss and detail each stage in the proposed system.

A. Experimental setup

The experimental setup was built and operated by Konecranes and the following experiment was repeated for three different synthetic fiber ropes; see Table I for the ropes' properties. First, the crane illustrated in Fig. 1 was set to continuously lift a payload of 5 metric tons in a controlled setting. The payload lifting height was approximately 5 meters and during a lifting cycle, the crane was stopped at the top and bottom (payload resting on the floor). After that, a circular camera array, comprised of three RGB cameras placed at 120° apart, was used to capture approximately 13 mm of the lifting rope. The camera framerate was selected such that subsequent rope images have roughly 1/3 spatial overlap, resulting in 20 meters of rope being photographed during a lifting cycle. Finally, the crane lifting and rope imaging steps were repeated for weeks to cover the ropes' lifespan; from new to unusable.

B. Data collection

The rope imaging experiment generated 4,984,000 high-resolution photos; each being tagged with a timestamp and the rope's imaged position. The raw photos were then screened for duplicates by discarding images that examined the same rope position. In other words, we ensured that images for the same rope position would be distinct by capturing different health

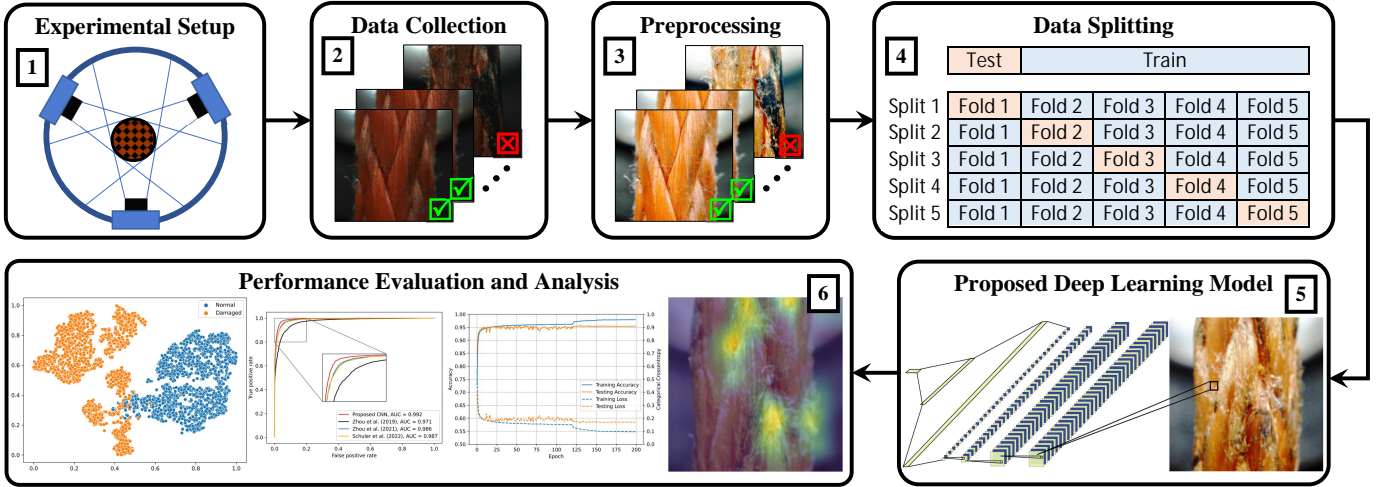


Fig. 2. The proposed vision-based damage detection system for synthetic fiber lifting ropes. The system is comprised of the following stages: (1) experimental setup with a three-camera circular array to capture rope images; (2) collection and annotation of the captured images; (3) preprocessing to enhance quality and down-sampling to reduce complexity; (4) data splitting into 5-fold training and testing sets; (5) training/testing the proposed deep learning model; and (6) evaluating and analyzing the system’s performance and computational complexity.

TABLE I
THE FIBER LIFTING ROPE PROPERTIES.

Diameter	12 mm
Material	Ultra high molecule weight polyethylene
Type	12-strand braided rope
Strength	15.4 metric tons (ISO 2307)
Weight	8.8 kg / 100 meters
Coating	Abrasion and ultra-violet resistance

conditions. This is important to avoid cross-contamination in data splits. After that, we selected 143,000 random samples and experts from Konecranes labeled them as *normal* or *damaged* according to the lifting rope health condition. Out of those images, 10,000 samples were labeled as damaged. Finally, to avoid data imbalance issues, we formed a balanced dataset containing 20,000 samples; 10,000 images from each class. The collected dataset is available from Konecranes and it was used under license for this study¹.

C. Preprocessing and data splitting

The annotated high-resolution rope images were down-sampled to $256 \times 256 \times 3$ pixels. After that, we enhanced the photos’ contrast via histogram equalization [26]; see Fig. 3 for a sample, and we standardized the pixel values to range between 0 and 1. Finally, the pre-processed images were randomly divided into five equally sized portions while maintaining class balance (5-fold stratified cross-validation); see stage 4 in Fig. 2. In other words, each split had 16,000 (8,000 damaged and 8,000 normal) and 4,000 (2,000 damaged and 2,000 normal) images for training and testing, respectively. Fig. 4 demonstrates samples of normal and damaged ropes



(a) Raw sample.

(b) Histogram equalized sample.

Fig. 3. Histogram equalization for an example rope image.

from the acquired dataset. By examining the images, one notes a significant variation in the clarity of the rope’s health state and in the severity of the damage. For example, Fig. 4a conveys a more damaged rope when compared to the one presented in Fig. 4e. However, the damage can also be minuscule without clear visual indications as presented in Fig. 4d. Finally, the dirt and oil stains found in most rope images present a challenge for any vision-based tool.

D. Proposed deep learning model

The collected rope images constitute an over-complete description for the rope as a whole; hence, the problem of damage detection reduces to classifying each image independently. We designed a lightweight CNN architecture to classify the fiber lifting rope images, and we tested different variants to find the best performing model.

The architecture design starts with a convolutional layer (3×3 kernel with ReLU activation) to extract preliminary feature maps from the input images. After that, those initial features are passed through a number of blocks each consisting of the following sequential elements: (1) convolutional layer to

¹Please contact Roope Mellanen at roope.mellanen@konecranes.com for data inquiry.

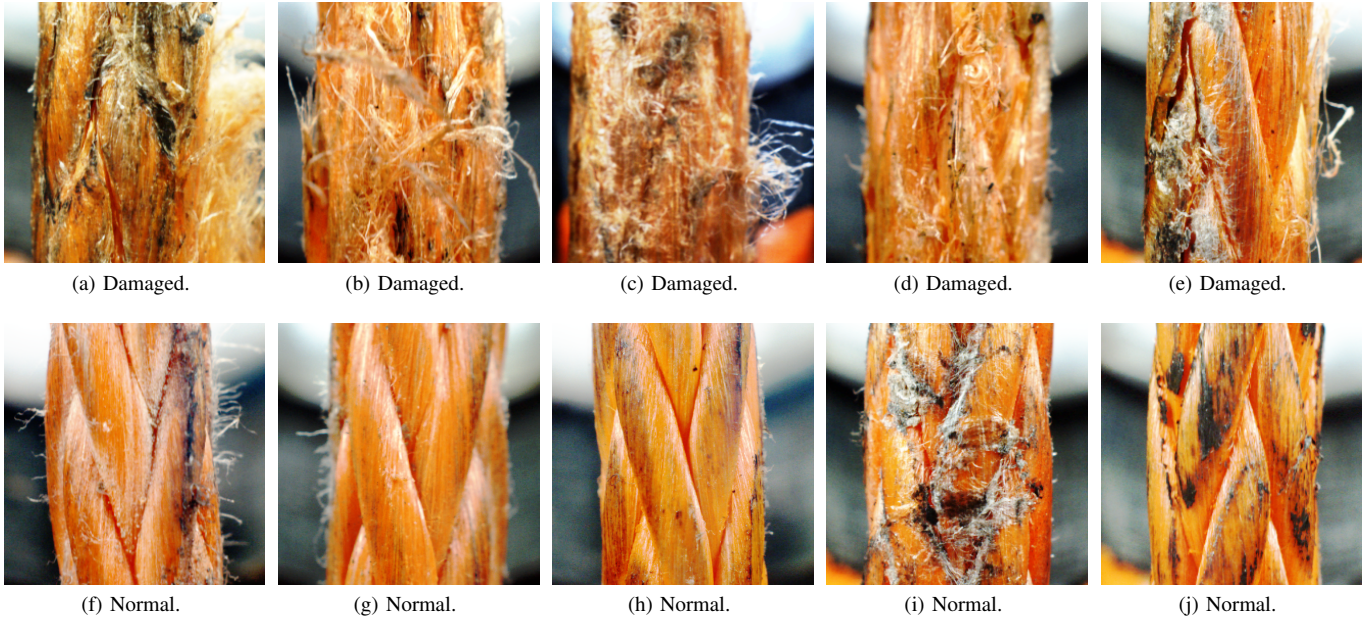


Fig. 4. Example images from the acquired dataset show significant variation in the severity and clarity of damages because of dirt and oil stains. The first row (a)-(e) show damaged ropes while the second row (f)-(j) present some healthy samples.

extract features (3×3 kernel with ReLU activation), (2) Max Pooling to down-sample the features (2×2 kernel), (3) and dropout to regularize the network by reducing the neurons' interdependent learning (0.4 rate). Finally, the learned abstractions are flattened and passed through a dropout layer (0.4 rate), a fully connected layer (20 nodes), another dropout layer (0.2 rate), and lastly, a binary classification layer with a Softmax activation function. In this work, 16 model variants were generated from this architecture by altering the number of blocks (1, 2, or 3), input image sizes (16×16 , 32×32 , or 64×64), and the input image color state (color or grayscale); see Appendix A for the model variants' structure and Table II for details on the variant that we selected for further analysis and comparison.

The models' training was performed for 200 epochs using an Adam optimizer [27] to minimize the cross-entropy loss regularized by a weight decay to reduce overfitting [28], [29], i.e.:

$$\mathcal{L} = -y \log(\hat{y}) - (1 - y) \log(1 - \hat{y}) + \lambda \|\mathbf{w}\|_2^2, \quad (1)$$

where \mathcal{L} denotes the regularized loss, y and \hat{y} are the true and predicted labels, respectively, $\lambda = 5 \times 10^{-4}$ is the selected L_2 regularization rate, and \mathbf{w} is the network's weight matrix [28]. Moreover, the training batch size was set to 32 and to ensure convergence the learning rate was decayed by [30]:

$$\eta(n) = \begin{cases} 10^{-3} & : n \leq 120 \\ 10^{-4} & : 120 < n \leq 150 \\ 10^{-5} & : 150 < n \leq 180 \\ 10^{-6} & : 180 < n \leq 200 \end{cases}, \quad (2)$$

where η is the learning rate and n is the epoch number. This training process was conducted for each model using the train set in each data split (five training sets). Additionally,

TABLE II
THE CNN9 MODEL VARIANT ARCHITECTURE.

Block #	Layer	Information	Output shape	Parameters
-	Conv	L_2 Kernel reg. = 0.0005 Kernel = 3×3 Activation = ReLU	$30 \times 30 \times 64$	1,792
1	Conv	L_2 Kernel reg. = 0.0005 Kernel = 3×3 Activation = ReLU	$28 \times 28 \times 64$	36,928
	MaxPool	Pool = 2×2	$14 \times 14 \times 64$	0
	Dropout	Rate = 0.4	$14 \times 14 \times 64$	0
2	Conv	L_2 Kernel reg. = 0.0005 Kernel = 3×3 Activation = ReLU	$12 \times 12 \times 64$	36,928
	MaxPool	Pool = 2×2	$6 \times 6 \times 64$	0
	Dropout	Rate = 0.4	$6 \times 6 \times 64$	0
	Flatten	-	2,304	0
-	Dropout	Rate = 0.4	2,304	0
	Dense	Activation = ReLU	20	46,100
	Dropout	Rate = 0.2	20	0
-	Dense	Activation = Softmax	2	42
Total number of parameters				121,790

apart from the generated variants, we also trained the following three baseline models for comparison; Zhou *et al.* (2019) [21], Zhou *et al.* (2021) [18], and Schuler *et al.* (2022) [31]. Detailed description on these models can be found in Appendixes B-D.

E. Performance evaluation and analysis

The trained models were evaluated using the test set in each data split (five test sets). Their performance was analyzed by various tools and metrics to quantify their fold-averaged detection, prediction, and misclassification outcomes.

1) *Classification*: we quantified the models' classification performance by accuracy, precision, recall, false positive rate (FPR), and the F1-score, i.e.:

$$\text{Accuracy} = \frac{TP + TN}{TP + TN + FP + FN}, \quad (3)$$

$$\text{Precision} = \frac{TP}{TP + FP}, \quad (4)$$

$$\text{Recall} = \frac{TP}{TP + FN}, \quad (5)$$

$$\text{FPR} = \frac{FP}{FP + TN}, \quad (6)$$

$$\text{F1-score} = 2 \left(\frac{\text{Precision} \times \text{Recall}}{\text{Precision} + \text{Recall}} \right), \quad (7)$$

where TP , TN , FP , and FN are true positives, true negatives, false positives, and false negatives, respectively (positive/negative denotes a damaged/normal rope).

Moreover, we used the area under the averaged receiver operating curve (AUC) and confusion matrices to fully characterize the classification quality. The AUC was computed by averaging linearly interpolated receiver operating curves.

2) *Prediction*: we assessed the models' predictive capacity using Gradient-weighted Class Activation Mapping (Grad-CAM) which uses gradients of the last convolutional layer to measure the relevance of the input image pixels for classification [32]. Specifically, Grad-CAM yields a distribution with high values for pixels that contributed more to the outcome. Furthermore, we utilized t-Distributed Stochastic Neighbor Embedding (t-SNE); a dimensionality reduction method that clusters similar high dimensional samples and departs dissimilar ones in two- or three-dimensional space [33]. In specific, given an array of learned features $\mathbf{x} = [\mathbf{x}_1, \mathbf{x}_2, \dots, \mathbf{x}_N]$, the similarity between features i and j can be measured by:

$$p_{ij} = \frac{p_{j|i} + p_{i|j}}{2N}, \quad (8)$$

$$p_{j|i} = \begin{cases} \frac{\exp(-\|\mathbf{x}_i - \mathbf{x}_j\|^2/2\sigma_i^2)}{\sum_{k \neq i} \exp(-\|\mathbf{x}_i - \mathbf{x}_k\|^2/2\sigma_i^2)} & : i \neq j \\ 0 & : i = j \end{cases}, \quad (9)$$

where p_{ij} is a probabilistic measure for the similarity between \mathbf{x}_i and \mathbf{x}_j , $\sum_{i,j} p_{ij} = 1$, $\sum_j p_{j|i} = 1$, and σ_i is the adaptive Gaussian kernel bandwidth. Now, t-SNE aims to learn the two- or three-dimensional map $\mathbf{y} = [\mathbf{y}_1, \mathbf{y}_2, \dots, \mathbf{y}_N]$ with a probabilistic similarity q_{ij} that resembles p_{ij} , i.e. [33]:

$$q_{ij} = \frac{(1 + \|\mathbf{y}_i - \mathbf{y}_j\|^2)^{-1}}{\sum_{k \neq l} (1 + \|\mathbf{y}_k - \mathbf{y}_l\|^2)^{-1}}. \quad (10)$$

The similarity matching between q_{ij} and p_{ij} in t-SNE is maximized by minimizing the Kullback–Leibler divergence of p_{ij} from q_{ij} via gradient descent, i.e.:

$$\min_{\mathbf{y}_i} \left(\sum_{i \neq j} p_{ij} \log \left(\frac{p_{ij}}{q_{ij}} \right) \right). \quad (11)$$

Both the Grad-CAM and t-SNE help in characterizing the models' predictive power when supplied with new data. In

other words, given large enough training samples, if the Grad-CAM and t-SNE show genuine learning and clear separability, one may infer the model adequacy for unseen samples.

3) *Misclassification*: visualizing the model's misclassified samples is paramount for interpretability and for outlining performance caps. Moreover, it enables a better understanding for the model's weaknesses and for identifying human errors in annotation. For example, by assuming some error in the labeling process, the performance of a genuine model will be limited, or capped, by the labels' quality.

F. Computational complexity

The complexity of the models was assessed by their total number of trainable parameters, required input image size, the models' memory size requirement, processing time, and their processing rate (frame rate). We analyzed their computational complexity by Monte-Carlo simulations where we fed the models with 4,000 test samples, predicted their health state (normal or damaged), and repeated the process ten times for validation. Note that this process does not include the imaging, data loading, nor preprocessing stages. It only quantifies the models' inference complexity. We used an Apple MacBook Pro with an ARM-based M1 Pro chip, 10-core CPU, integrated 16-core GPU, 16-core neural engine, and 16 GB of RAM. The experiments' codes were written in Python 3.9.7 using Tensorflow 2.7.0 and are publicly available.

III. RESULTS AND DISCUSSION

A. Model selection

The best model, out of the 16 generated variants, was selected based on its ability to balance between precision and recall with minimum computational requirements. By examining the results in Table III, one notes that the model variants CNN9 and CNN15 yield the highest 5-fold averaged precision/recall balance (96.5% average). Besides, they are the top-2 models in terms of accuracy, precision, F1-score, and AUC. Nevertheless, due to the apparent disparity in computational resources (input image sizes: $32 \times 32 \times 3$ v.s. $64 \times 64 \times 3$), we opted for model CNN9 and used it for further analysis and comparison. Note that "Proposed CNN" refers to the CNN9 variant in the remaining of this paper.

B. Performance analysis

Fig. 5 compares the training and testing accuracy/loss curves (averaged over the data splits) of the proposed CNN to the three baseline models. The results show the curves converging successfully after epoch 150, and the learning rate decay, scheduled at epoch 151, has ensured stability by suppressing perturbation. This indicates that the training phase was executed long enough and was not terminated prematurely. Moreover, by examining the difference between the training and testing accuracy/loss curves one notes that the three baseline models exhibit further overfitting when compared to the proposed network, with Schuler *et al.* (2022) being the extreme case, followed by Zhou *et al.* (2019), and lastly, Zhou

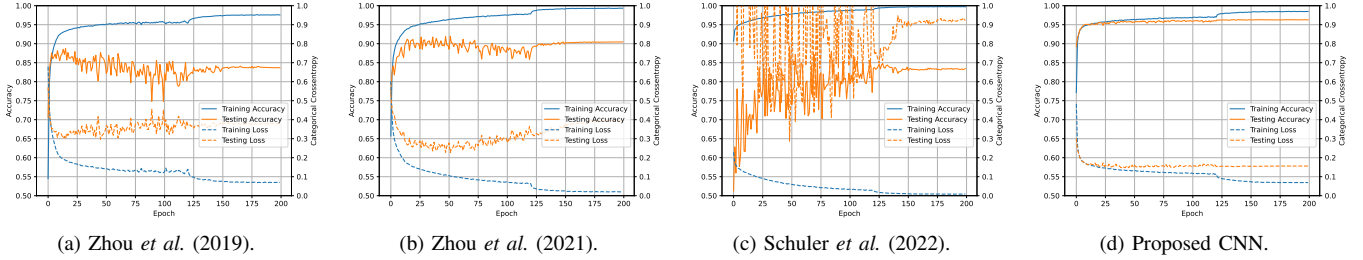


Fig. 5. Comparing the models' training and testing accuracy/loss curves averaged over the data splits in solid/dotted lines.

TABLE III

THE PROPOSED CNN MODEL VARIANTS' TESTING PERFORMANCE IN TERMS OF ACCURACY, PRECISION, RECALL, FNR, F1-SCORE, AND AUC. THE RESULTS ARE SUMMARIZED BY THEIR 5-FOLD AVERAGED PERCENTAGES, \pm STANDARD DEVIATIONS, AND THE SELECTED BEST MODEL VARIANT IS HIGHLIGHTED IN BOLD.

Variant #	Accuracy	Precision	Recall	FNR	F1-score	AUC
CNN1	94.8 \pm 0.4	93.9 \pm 0.2	95.9 \pm 0.7	4.1 \pm 0.7	94.9 \pm 0.4	98.4 \pm 0.1
CNN2	94.0 \pm 0.5	93.8 \pm 1.0	94.2 \pm 0.8	5.8 \pm 0.8	94.0 \pm 0.4	98.1 \pm 0.2
CNN3	96.0 \pm 0.4	95.8 \pm 0.3	96.3 \pm 0.8	3.7 \pm 0.8	96.1 \pm 0.4	99.1 \pm 0.1
CNN4	95.7 \pm 0.3	95.2 \pm 0.7	96.3 \pm 0.5	3.7 \pm 0.5	95.7 \pm 0.3	99.0 \pm 0.1
CNN5	95.2 \pm 0.2	95.0 \pm 0.3	95.5 \pm 0.5	4.5 \pm 0.5	95.2 \pm 0.2	98.5 \pm 0.1
CNN6	95.7 \pm 0.3	95.1 \pm 0.5	96.4 \pm 0.1	3.6 \pm 0.1	95.8 \pm 0.3	98.8 \pm 0.1
CNN7	94.3 \pm 0.6	91.7 \pm 1.5	97.5 \pm 0.7	2.5 \pm 0.7	94.5 \pm 0.5	98.6 \pm 0.1
CNN8	96.4 \pm 0.3	95.8 \pm 0.4	97.0 \pm 0.4	3.0 \pm 0.4	96.4 \pm 0.3	99.0 \pm 0.2
CNN9	96.4 \pm 0.5	95.8 \pm 0.5	97.2 \pm 0.8	2.8 \pm 0.8	96.5 \pm 0.5	99.2 \pm 0.1
CNN10	96.1 \pm 0.3	95.5 \pm 0.2	96.9 \pm 0.6	3.1 \pm 0.6	96.2 \pm 0.3	99.1 \pm 0.2
CNN11	95.0 \pm 0.1	94.6 \pm 0.5	95.5 \pm 0.4	4.5 \pm 0.4	95.0 \pm 0.1	98.4 \pm 0.1
CNN12	95.9 \pm 0.2	95.2 \pm 0.5	96.7 \pm 0.5	3.3 \pm 0.5	95.9 \pm 0.2	98.8 \pm 0.2
CNN13	95.4 \pm 0.5	93.7 \pm 1.0	97.3 \pm 0.8	2.7 \pm 0.8	95.4 \pm 0.4	98.9 \pm 0.1
CNN14	96.2 \pm 0.4	95.9 \pm 0.6	96.5 \pm 0.4	3.5 \pm 0.4	96.2 \pm 0.4	99.0 \pm 0.2
CNN15	96.5 \pm 0.3	95.8 \pm 0.5	97.2 \pm 0.3	2.8 \pm 0.3	96.5 \pm 0.3	99.1 \pm 0.2
CNN16	96.4 \pm 0.2	94.9 \pm 0.4	98.0 \pm 0.5	2.0 \pm 0.5	96.4 \pm 0.2	99.2 \pm 0.1

et al. (2021). We argue that this is caused by the unnecessary high number of parameters which hinder generalization.

The models' testing performance for detecting damaged rope images is demonstrated in Table IV and Fig. 6. The measures in Table IV show that the Zhou *et al.* (2021) model has the highest recall at 97.9%, which is the most important metric in order to prevent accidents. However, its precision, at 90.3%, is relatively low suggesting that the model labels most rope images as damaged, making it unpractical for a real-life setting. Moreover, both the Schuler *et al.* (2022) and the proposed models yield similar recall levels (97.1% and 97.2%, respectively). Nevertheless, the proposed CNN results in higher accuracy, precision, and F1-score with 2.3, 4.2, and 2.2 percentage point gains, respectively. In addition, it demonstrates a better precision/recall trade-off, which is reflected by the averaged ROC curve in Fig. 6 along with its AUC value (99.2%). Finally, the results suggest that the Zhou *et al.* (2019) and Schuler *et al.* (2022) models are not the best in any of the six metrics.

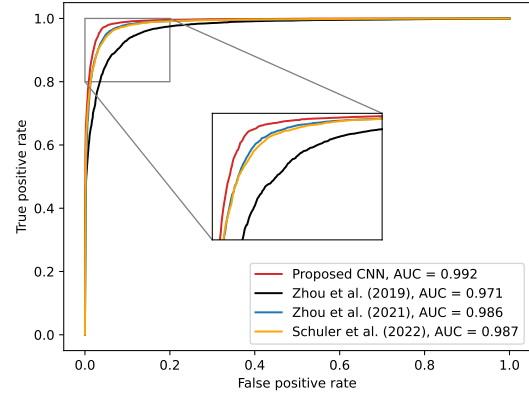


Fig. 6. The models' 5-fold averaged ROC curves alongside their computed AUC values. The corner portion is magnified to ease visualization.

C. Computational complexity analysis

Table V summarizes the complexity analysis results which indicate that the proposed model is the fastest one requiring approximately 19 milliseconds per input image and running in real-time at 54 fps. Nonetheless, it is important to note that Zhou *et al.* (2019) and (2021) models are comparatively fast, but the Schuler *et al.* (2022) operates below real-time at 12 fps. Besides, the listed prediction speeds could be further improved by running them in C++. However, the most notable and important difference is the proposed model's lighter memory footprint. In specific, our model accepts small-sized images and requires less disk space for storage. These advantages can lead to savings in equipment and operational costs, improve latency, and mitigate privacy issues by not using cloud services.

D. The Grad-CAM and t-SNE analysis

The Grad-CAM and t-SNE results are depicted in Figs. 7 and 8, respectively. In Fig. 7, we generated the Grad-CAM heatmap for two example images showing damaged ropes that were correctly classified by the proposed model. The results show that our CNN model is indeed focusing on the intuitively relevant parts of the input image, which are the broken strands. One also notes that the network does not focus on the ropes' oil and dirt residue as demonstrated in Fig. 7b. This suggests genuine learning by the model and robustness to environmental

TABLE IV

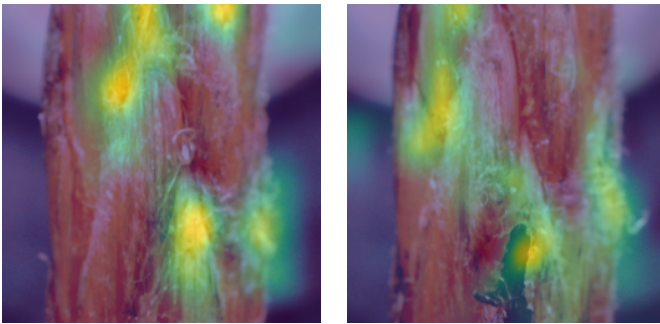
THE MODELS' TESTING PERFORMANCE IN TERMS OF TP , TN , FP , AND FN PRESENTED IN A CONFUSION MATRIX FASHION, ALONG WITH THEIR ACCURACY, PRECISION, RECALL, FNR , AND $F1$ -SCORE. THE CONFUSION MATRIX ENTRIES ARE ACCUMULATED FROM THE 5-FOLDS, THE REMAINING RESULTS ARE SUMMARIZED BY THEIR 5-FOLD AVERAGE PERCENTAGES, \pm STANDARD DEVIATIONS, AND THE BEST OUTCOMES ARE SHOWN IN BOLD.

	Zhou <i>et al.</i> (2019)		Zhou <i>et al.</i> (2021)		Schuler <i>et al.</i> (2022)		Proposed CNN	
TN FP	8,641	1,359	8,933	1,067	9,107	893	9,570	430
FN TP	355	9,645	215	9,785	293	9,707	281	9,719
Accuracy	91.4 \pm 2.7		93.6 \pm 1.7		94.1 \pm 1.1		96.4 \pm 0.5	
Precision	87.7 \pm 3.1		90.3 \pm 3.5		91.6 \pm 2.2		95.8 \pm 0.5	
Recall	96.4 \pm 2.5		97.9 \pm 1.0		97.1 \pm 1.0		97.2 \pm 0.8	
FNR	3.6 \pm 2.5		2.2 \pm 1.0		2.9 \pm 1.0		2.8 \pm 0.8	
F1-score	91.9 \pm 2.6		93.9 \pm 1.53		94.3 \pm 0.9		96.5 \pm 0.5	
AUC	97.1 \pm 2.4		98.6 \pm 0.1		98.7 \pm 0.2		99.2 \pm 0.1	

TABLE V

THE MODELS' COMPUTATIONAL COMPLEXITY IN TERMS OF THEIR TOTAL NUMBER OF PARAMETERS, INPUT IMAGE SIZE REQUIREMENT, MODEL SIZE, AVERAGE PROCESSING TIME \pm STANDARD DEVIATION IN MILLISECONDS, AVERAGE PROCESSING RATE IN FPS, AND AVERAGE TRAINING TIME PER EPOCH \pm STANDARD DEVIATION IN SECONDS.

	Zhou <i>et al.</i> (2019)	Zhou <i>et al.</i> (2021)	Schuler <i>et al.</i> (2022)	Proposed CNN
No. of parameters	12.8 M	498 K	371 K	122 K
Image size	3.57 KB	7.46 KB	2.84 KB	2.84 KB
Model size	154 MB	6.28 MB	18.5 MB	1.73 MB
Processing time	20.7 \pm 4.2 ms	20.1 \pm 4.2 ms	82.7 \pm 18.0 ms	18.7 \pm 3.6 ms
Processing rate	48.3 fps	49.8 fps	12.1 fps	53.5 fps
Training time per epoch	17.7 \pm 0.39 s	18.3 \pm 0.11 s	183.4 \pm 4.47 s	14.8 \pm 0.06 s



(a) Example 1.

(b) Example 2.

Fig. 7. The proposed CNN Grad-CAM heatmaps for two correctly classified damaged ropes. The heatmaps indicate the model's adequacy by focusing on the pixels that are relevant for detecting damage. We used the model's last convolutional layer features as input to the Grad-Cam algorithm.

and operational conditions. However, it is important to note that the CNN still slightly focuses on the image background. Moreover, the t-SNE results in Fig. 8 demonstrate good class separation, but they also show a need for verifying some ground-truth labels. In specific, the t-SNE shows few rope images labeled as normal within the damaged rope support.

E. Misclassifications

Two example prediction errors by our CNN are presented in Fig. 9. The rope in Fig. 9a is labeled as damaged, but

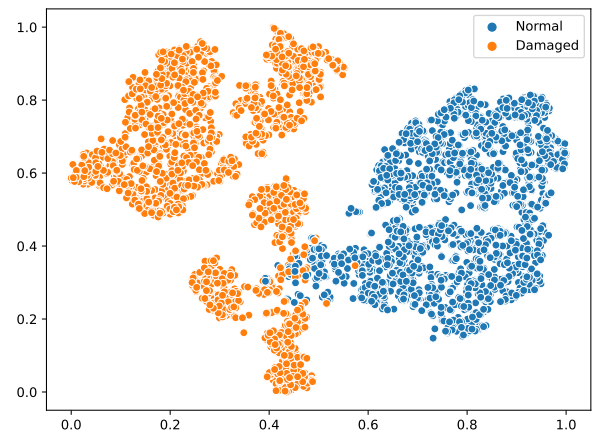
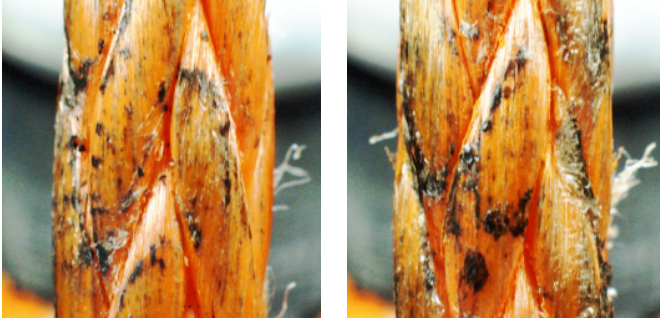


Fig. 8. The proposed CNN t-SNE results showing good separation between the two classes. We used the model's last layer features (FC[20] in Table A.1) as input to the t-SNE algorithm.

predicted as normal, while the one in Fig. 9b is labeled as normal, but predicted as damaged. Such instances pose a challenge for the system because they are clearly in between the two classes; they are slightly worn with a few broken strings, but strictly not damaged, according to our experts. Despite that, these ropes are not likely to break at these spots and they would be classified as damaged after more wear. Moreover, the similarities between the two images suggest



(a) True: Damaged, Predicted: Normal. (b) True: Normal, Predicted: Damaged.
 Fig. 9. Two example misclassification samples by the proposed CNN.

possible annotation errors which may prevent the proposed model from reaching its full potential. Nonetheless, human errors are expected, and the model outcome still shows good potential and applicability.

IV. CONCLUSIONS

Damaged lifting ropes are a major safety hazard in manufacturing, cargo loading/unloading, and construction because they can lead to serious accidents, injuries, and financial losses. The visual inspection of damage in synthetic lifting ropes is a time-consuming task, interrupts operation, and may result in the premature disposal of ropes. Therefore, combining computer vision and deep learning techniques is intuitive for automation and advancement.

This work presents a novel vision-based deep learning solution for detecting damage in fiber lifting rope images. First, we built a three-camera circular array apparatus to photograph the rope’s surface. Afterward, the rope surface images were collected in a database, annotated by experts, preprocessed to improve contrast, and split into train and test sets in a 5-fold cross-validation fashion. Moreover, we systematically designed a CNN-based model to classify damaged rope images, evaluated its detection and prediction performance using various tools, and compared it to three different baseline models. Additionally, we analyzed its computational complexity in terms of processing time and memory footprint. In summary, the results indicated various performance and computational advantages for using the proposed system when compared to similar solutions. Specifically, the system testing yielded 96.4% accuracy, 95.8% precision, 97.2% recall, 96.5% F1-score, 99.2% AUC, and a significant generalization capability. Besides, it runs at 54 fps, occupies 1.7 MB in memory, and requires low-resolution input images; thus, making the proposed system a real-time lightweight solution. The developed system was also found robust to various environmental and operational conditions e.g., oil residue and dust.

The proposed model’s main drawback is not determining the rope health state as a whole but assessing each image individually. Besides, the system’s output is binary and does not directly communicate the rope’s health condition. These limitations propose extending the developed solution in various ways such as: (1) collecting a larger training dataset with different rope sizes and types to improve generalization; (2)

investigating other machine learning solutions and techniques; (3) including the cost of the imaging apparatus in the design process, e.g., using cheaper cameras; (4) extending the model’s output to multiple classes e.g., normal, worn, and damaged, or to a continuous score indicating the rope’s health condition (regression); and (5) incorporating the proposed solution to automate or recommend spare-part ordering.

ACKNOWLEDGMENT

We would like to thank Konecranes and Juhani Kerovuori for their collaboration on this project.

APPENDIX A

THE PROPOSED MODEL VARIANTS

Table A.1 summarizes the proposed CNN model variants’ architecture for implementation. The variants were generated by altering the number of blocks, input image sizes, and input image color state.

APPENDIX B

THE ZHOU ET AL. (2019) AND (2021) MODELS

The proposed damage detection solution was compared to the Zhou *et al.* (2019) [21] and Zhou *et al.* (2021)² [18] models in terms of performance and computational requirements. These models were originally designed to detect surface damage in steel wire rope images with high performance. Although the rope material is different from our experiments (steel v.s. fiber), these detection models are still suitable for adoption due to the similarity between the two problems; they both deal with detecting damaged yarns or strands in rope images. The Zhou *et al.* (2019) and (2021) architectures accept grayscale input images of size 64×64 and 96×96 , and produce outputs of size 3 and 2, respectively. In this work, we changed the Zhou *et al.* (2019) output shape to 2 in order to match our problem definition, and we added six dropout layers (0.5 rate) to mitigate overfitting. Moreover, we increased the Zhou *et al.* (2021) original two dropout rates to 0.6 and added three more dropout layers to avoid overfitting.

APPENDIX C

THE SCHULER ET AL. (2022) MODEL

The proposed damage detection solution was also compared to the Schuler *et al.* (2022)³ [31] model; a highly efficient CNN-based classifier. The Schuler *et al.* (2022) model was designed in a clever manner to reduce the number of required parameters while maintaining high performance; the accuracy drop was 2% for a 55% reduction in parameters when tested on the CIFAR-10 dataset [31]. Therefore, we opted for this architecture for comparison because it is aligned with our design requirements; high efficiency and performance. The Schuler *et al.* (2022) model accepts colored input images of size $32 \times 32 \times 3$, and in this work, we used its original implementation. Nonetheless, we reduced its output size from 10 to 2 in order to match our problem definition, and added dropout layers (0.4 rate) to minimize overfitting.

²The adopted Zhou *et al.* (2021) model is named WRIPDCNN1 in [18].

³The adopted Schuler *et al.* (2022) model is named kDenseNet-BC L100 12ch in [31].

TABLE A.1

THE PROPOSED CNN MODEL VARIANTS' STRUCTURE. $NC[k \times k]$ DENOTES A CONVOLUTIONAL LAYER WITH N KERNELS EACH OF SIZE $k \times k$, $MP[k \times k]$ IS MAX POOLING WITH A $k \times k$ KERNEL, $D[k]$ IS DROPOUT WITH RATE k , AND $FC[N]$ IS A FULLY CONNECTED LAYER WITH N NODES. THE SELECTED MODEL VARIANT (CNN9) IS HIGHLIGHTED IN BOLD.

Variant #	Input Image Size	Preliminary	First Block	Second Block	Third Block	Fully Connected
CNN1	16x16x1	64C[3x3]	64C[3x3]-MP[2x2]-D[0.4]	-	-	Flatten-D[0.4]-FC[20]-D[0.2]-Output[2]
CNN2	16x16x1	64C[3x3]	64C[3x3]-MP[2x2]-D[0.4]	64C[3x3]-MP[2x2]-D[0.4]	-	Flatten-D[0.4]-FC[20]-D[0.2]-Output[2]
CNN3	16x16x3	64C[3x3]	64C[3x3]-MP[2x2]-D[0.4]	-	-	Flatten-D[0.4]-FC[20]-D[0.2]-Output[2]
CNN4	16x16x3	64C[3x3]	64C[3x3]-MP[2x2]-D[0.4]	64C[3x3]-MP[2x2]-D[0.4]	-	Flatten-D[0.4]-FC[20]-D[0.2]-Output[2]
CNN5	32x32x1	64C[3x3]	64C[3x3]-MP[2x2]-D[0.4]	-	-	Flatten-D[0.4]-FC[20]-D[0.2]-Output[2]
CNN6	32x32x1	64C[3x3]	64C[3x3]-MP[2x2]-D[0.4]	64C[3x3]-MP[2x2]-D[0.4]	-	Flatten-D[0.4]-FC[20]-D[0.2]-Output[2]
CNN7	32x32x1	64C[3x3]	64C[3x3]-MP[2x2]-D[0.4]	64C[3x3]-MP[2x2]-D[0.4]	64C[3x3]-MP[2x2]-D[0.4]	Flatten-D[0.4]-FC[20]-D[0.2]-Output[2]
CNN8	32x32x3	64C[3x3]	64C[3x3]-MP[2x2]-D[0.4]	-	-	Flatten-D[0.4]-FC[20]-D[0.2]-Output[2]
CNN9	32x32x3	64C[3x3]	64C[3x3]-MP[2x2]-D[0.4]	64C[3x3]-MP[2x2]-D[0.4]	-	Flatten-D[0.4]-FC[20]-D[0.2]-Output[2]
CNN10	32x32x3	64C[3x3]	64C[3x3]-MP[2x2]-D[0.4]	64C[3x3]-MP[2x2]-D[0.4]	64C[3x3]-MP[2x2]-D[0.4]	Flatten-D[0.4]-FC[20]-D[0.2]-Output[2]
CNN11	64x64x1	64C[3x3]	64C[3x3]-MP[2x2]-D[0.4]	-	-	Flatten-D[0.4]-FC[20]-D[0.2]-Output[2]
CNN12	64x64x1	64C[3x3]	64C[3x3]-MP[2x2]-D[0.4]	64C[3x3]-MP[2x2]-D[0.4]	-	Flatten-D[0.4]-FC[20]-D[0.2]-Output[2]
CNN13	64x64x1	64C[3x3]	64C[3x3]-MP[2x2]-D[0.4]	64C[3x3]-MP[2x2]-D[0.4]	64C[3x3]-MP[2x2]-D[0.4]	Flatten-D[0.4]-FC[20]-D[0.2]-Output[2]
CNN14	64x64x3	64C[3x3]	64C[3x3]-MP[2x2]-D[0.4]	-	-	Flatten-D[0.4]-FC[20]-D[0.2]-Output[2]
CNN15	64x64x3	64C[3x3]	64C[3x3]-MP[2x2]-D[0.4]	64C[3x3]-MP[2x2]-D[0.4]	-	Flatten-D[0.4]-FC[20]-D[0.2]-Output[2]
CNN16	64x64x3	64C[3x3]	64C[3x3]-MP[2x2]-D[0.4]	64C[3x3]-MP[2x2]-D[0.4]	64C[3x3]-MP[2x2]-D[0.4]	Flatten-D[0.4]-FC[20]-D[0.2]-Output[2]

APPENDIX D

BASELINE TRAINING AND EVALUATION SETTINGS

The baseline models' training followed the same procedure described in section II-D using the train set in each data split (five training sets), but with no weight decay. Besides, their performance was evaluated using the test set in each data split (five test sets) and quantified by the measures described in section II-E. Note that the Schuler model has caused out-of-memory issues when trained with a batch size above 32 using the equipment described in section II-F.

REFERENCES

- [1] Z. Liu, K. Xie, L. Li, and Y. Chen, "A paradigm of safety management in industry 4.0," *Systems Research and Behavioral Science*, vol. 37, no. 4, pp. 632–645, 2020.
- [2] I. Ahmed, G. Jeon, and F. Piccialli, "From Artificial Intelligence to Explainable Artificial Intelligence in Industry 4.0: A Survey on What, How, and Where," *IEEE Transactions on Industrial Informatics*, vol. 18, no. 8, pp. 5031–5042, 2022.
- [3] Z. Xu and J. H. Saleh, "Machine learning for reliability engineering and safety applications: Review of current status and future opportunities," *Reliability Engineering & System Safety*, vol. 211, p. 107530, 2021.
- [4] T. Jalonen, F. Laakom, M. Gabbouj, and T. Puoskari, "Visual Product Tracking System Using Siamese Neural Networks," *IEEE Access*, vol. 9, pp. 76 796–76 805, 2021.
- [5] J. Lee, I. Phillips, and Z. Lynch, "Causes and prevention of mobile crane-related accidents in South Korea," *International Journal of Occupational Safety and Ergonomics*, pp. 469–478, 2020.
- [6] Konecranes, "Smart cranes by Konecranes," *Steel Times International*, vol. 43, no. 8, p. 32, Nov 2019. [Online]. Available: <https://www.proquest.com/scholarly-journals/smart-cranes-konecranes/docview/2376650666/se-2>
- [7] KONECRANES, *KONECRANES S-Series Crane: The new standard in lifting*. [Online]. Available: https://www.konecranes.com/sites/default/files/2020-12/S_series_crane_flyer_en_Konecranes_2019_0.pdf
- [8] I. Mupende, F. Lukasch, and P. Tonnier, "Experiences with Fibre Ropes as Hoist Ropes in Crane Applications," *inoTRAC Journal*, vol. 1, pp. 9–18, Dec. 2020.
- [9] *ISO 9554:2019 Fibre ropes — General specifications*, Sustainable Development Goals Std. [Online]. Available: <https://www.iso.org/standard/72077.html>
- [10] A. Schmierer and M. Golder, "Investigating the Lifetime of Fibre Ropes," *inoTRAC Journal*, vol. 1, pp. 1–8, Dec. 2020.
- [11] S. Falconer, A. Gromsrud, E. Oland, and G. Grasmø, "Preliminary Results on Condition Monitoring of Fiber Ropes using Automatic Width and Discrete Length Measurements," in *Annual Conference of the PHM Society*, vol. 9, no. 1, 2017.
- [12] M. Yousri, G. Jacobs, and S. Neumann, "Impact of fiber versus steel ropes on the lifetime of crane winches," *Modeling, Identification and Control*, vol. 41, no. 3, pp. 129–139, 2020.
- [13] G. P. Foster, "Advantages of Fiber Rope Over Wire Rope," *Journal of Industrial Textiles*, vol. 32, no. 1, pp. 67–75, 2002.
- [14] E. Oland, R. Schlanbusch, and S. Falconer, "Condition Monitoring Technologies for Synthetic Fiber Ropes—a Review," *International Journal of Prognostics and Health Management*, vol. 8, no. 2, 2017.
- [15] R. Schlanbusch, E. Oland, and E. R. Bechhoefer, "Condition Monitoring Technologies for Steel Wire Ropes—A Review," *International Journal of Prognostics and Health Management*, vol. 8, no. 1, 2017.
- [16] P. Zhou, G. Zhou, Z. Zhu, Z. He, X. Ding, and C. Tang, "A Review of Non-Destructive Damage Detection Methods for Steel Wire Ropes," *Applied Sciences*, vol. 9, no. 13, 2019.
- [17] X. Huang, Z. Liu, X. Zhang, J. Kang, M. Zhang, and Y. Guo, "Surface damage detection for steel wire ropes using deep learning and computer vision techniques," *Measurement*, vol. 161, p. 107843, 2020.
- [18] P. Zhou, G. Zhou, H. Wang, D. Wang, and Z. He, "Automatic Detection of Industrial Wire Rope Surface Damage Using Deep Learning-Based Visual Perception Technology," *IEEE Transactions on Instrumentation and Measurement*, vol. 70, pp. 1–11, 2021.
- [19] S. Falconer, E. Nordgård-Hansen, and G. Grasmø, "Computer vision and thermal monitoring of HMPE fibre rope condition during CBOS testing," *Applied Ocean Research*, vol. 102, p. 102248, 2020.
- [20] P. Zhou, G. Zhou, Z. Zhu, C. Tang, Z. He, W. Li, and F. Jiang, "Health Monitoring for Balancing Tail Ropes of a Hoisting System Using a Convolutional Neural Network," *Applied Sciences*, vol. 8, no. 8, 2018.
- [21] Z. Ping, Z. Gongbo, L. Yingming, and H. Zhenzhi, "Surface defect detection for wire ropes based on deep convolutional neural network," in *2019 14th IEEE International Conference on Electronic Measurement Instruments (ICEMI)*, 2019, pp. 855–860.
- [22] P. Zhou, G. Zhou, Z. He, C. Tang, Z. Zhu, and W. Li, "A novel texture-based damage detection method for wire ropes," *Measurement*, vol. 148, p. 106954, 2019.
- [23] P. Zhou, G. Zhou, Y. Li, Z. He, and Y. Liu, "A Hybrid Data-Driven Method for Wire Rope Surface Defect Detection," *IEEE Sensors Journal*, vol. 20, no. 15, pp. 8297–8306, 2020.
- [24] G. Zhang, Z. Tang, J. Zhang, and W. Gui, "Convolutional Autoencoder-Based Flaw Detection for Steel Wire Ropes," *Sensors*, vol. 20, no. 22, 2020.

- [25] M. Verhelst and B. Moons, "Embedded Deep Neural Network Processing: Algorithmic and Processor Techniques Bring Deep Learning to IoT and Edge Devices," *IEEE Solid-State Circuits Magazine*, vol. 9, no. 4, pp. 55–65, 2017.
- [26] W. A. Mustafa and M. A. Kader, "A Review of Histogram Equalization Techniques in Image Enhancement Application," *Journal of Physics: Conference Series*, vol. 1019, p. 012026, June 2018.
- [27] D. P. Kingma and J. Ba, "Adam: A method for stochastic optimization," *arXiv preprint arXiv:1412.6980*, 2014. [Online]. Available: <https://doi.org/10.48550/arXiv.1412.6980>Focustolearnmore
- [28] Z. Zhang and M. Sabuncu, "Generalized Cross Entropy Loss for Training Deep Neural Networks with Noisy Labels," in *Advances in Neural Information Processing Systems*, S. Bengio, H. Wallach, H. Larochelle, K. Grauman, N. Cesa-Bianchi, and R. Garnett, Eds., vol. 31. Curran Associates, Inc., 2018. [Online]. Available: <https://proceedings.neurips.cc/paper/2018/hash/f2925f97bc13ad2852a7a551802feca0-Abstract.html>
- [29] T. Van Laarhoven, "L2 regularization versus batch and weight normalization," *arXiv preprint arXiv:1706.05350*, 2017.
- [30] R. Ge, S. M. Kakade, R. Kidambi, and P. Netrapalli, "The Step Decay Schedule: A Near Optimal, Geometrically Decaying Learning Rate Procedure For Least Squares," in *Advances in Neural Information Processing Systems*, H. Wallach, H. Larochelle, A. Beygelzimer, F. d'Alché-Buc, E. Fox, and R. Garnett, Eds., vol. 32. Curran Associates, Inc., 2019. [Online]. Available: <https://proceedings.neurips.cc/paper/2019/file/2f4059ce1227f021edc5d9c6f0f17dc1-Paper.pdf>
- [31] J. P. Schwarz, S. Romani, M. Abdel-nasser, H. Rashwan, and D. Puig, "Grouped Pointwise Convolutions Reduce Parameters in Convolutional Neural Networks," *Mendel*, vol. 28, pp. 23–31, 06 2022.
- [32] R. R. Selvaraju, M. Cogswell, A. Das, R. Vedantam, D. Parikh, and D. Batra, "Grad-CAM: Visual Explanations From Deep Networks via Gradient-Based Localization," in *Proceedings of the IEEE International Conference on Computer Vision (ICCV)*, Oct. 2017, pp. 618–626. [Online]. Available: https://openaccess.thecvf.com/content_iccv_2017/html/Selvaraju_Grad-CAM_Visual_Explanations_ICCV_2017_paper.html
- [33] L. van der Maaten and G. Hinton, "Visualizing data using t-SNE," *Journal of Machine Learning Research*, vol. 9, no. 86, pp. 2579–2605, 2008. [Online]. Available: <https://jmlr.org/papers/v9/vandermaaten08a.html>



Tuomas Jalonen received the B.Sc. and M.Sc. degrees in mechanical engineering from Tampere University, Finland, in 2017 and 2019, respectively. He is currently pursuing the Ph.D. degree with the Faculty of Information Technology and Communication Sciences of Tampere University, Finland. His research interest includes the development of machine learning applications for manufacturing.



Mohammad Al-Sa'd (Senior Member, IEEE) received his B.Sc. and M.Sc. degrees in Electrical Engineering from Qatar University, Qatar, in 2012 and 2016 respectively, and his PhD degree in Electrical Engineering and Computing Sciences from Tampere University, Finland, in 2022. He specialized in signal processing and he is currently pursuing his postdoctoral fellowship at the Department of Neuroscience, University of Helsinki, Finland. He has served as a technical reviewer for several journals, including IEEE transactions on signal processing, digital signal processing, signal processing, biomedical signal processing and control, and IEEE Access. His research interests include time-frequency signal theory, machine learning, electroencephalogram analysis and processing, information flow and theory, signal modeling, and optimization.



Roope Mellanen received the B.Sc. and M.Sc. degrees in automation from Tampere University of Technology, Finland, in 2016 and 2018, respectively. He is currently working as a Research Specialist for Konecranes Corporation. His research interest includes machine learning, computer vision, and signal processing and analytics.



Serkan Kiranyaz (Senior Member, IEEE) is a Professor with Qatar University, Doha, Qatar. He published two books, five book chapters, more than 80 journal articles in high impact journals, and 100 articles in international conferences. He made contributions on evolutionary optimization, machine learning, bio-signal analysis, computer vision with applications to recognition, classification, and signal processing. He has coauthored the articles which have nominated or received the "Best Paper Award" in ICIP 2013, ICPR 2014, ICIP 2015, and IEEE Transactions on Signal Processing (TSP) 2018. He had the most-popular articles in the years 2010 and 2016, and most-cited article in 2018 in IEEE Transactions on Biomedical Engineering. From 2010 to 2015, he authored the 4th most-cited article of the Neural Networks journal. His research team has won the second and first places in PhysioNet Grand Challenges 2016 and 2017, among 48 and 75 international teams, respectively. His theoretical contributions to advance the current state of the art in modeling and representation, targeting high long-term impact, while algorithmic, system level design and implementation issues target medium and long-term challenges for the next five to ten years. He in particular aims at investigating scientific questions and inventing cutting-edge solutions in "personalized biomedicine" which is in one of the most dynamic areas where science combines with technology to produce efficient signal and information processing systems.



Moncef Gabbouj (Fellow Member, IEEE) received the B.S. degree from Oklahoma State University, Stillwater, OK, USA, in 1985, and the M.S. and Ph.D. degrees from Purdue University, in 1986 and 1989, respectively, all in electrical engineering. He is a Professor of signal processing with the Department of Computing Sciences, Tampere University, Tampere, Finland. He was an Academy of Finland Professor from 2011 to 2015. His research interests include big data analytics, multimedia content-based analysis, indexing and retrieval, artificial intelligence, machine learning, pattern recognition, nonlinear signal and image processing and analysis, voice conversion, and video processing and coding. Dr. Gabbouj is a member of the Academia Europaea and the Finnish Academy of Science and Letters. He is the past Chairman of the IEEE CAS TC on DSP and the Committee Member of the IEEE Fourier Award for Signal Processing. He served as an Associate Editor and the Guest Editor of many IEEE, and international journals and a Distinguished Lecturer for the IEEE CASS. He is the Finland Site Director of the NSF IUCRC funded Center for Visual and Decision Informatics (CVDI) and leads the Artificial Intelligence Research Task Force of the Ministry of Economic Affairs and Employment funded Research Alliance on Autonomous Systems (RAAS).